Electronic Supplementary Material (ESI) for Journal of Materials Chemistry A.

Supporting Information

A Cost Effective, Highly Porous, Manganese Oxide/Carbon Supercapacitor Material with High Rate Capability

Rongfang Wang, Yuanyuan Ma, Hui Wang, Julian Key, Dan Brett, Shan Ji, Shibin Yin and Pei Kang shen

Experimental Details

Synthesis of Macrporous Mn_2O_3/Carbon. All reagents were of analytic grade and ultrapure water was used throughout the experiments. Porous Mn_2O_3/Carbon (Mn_2O_3/C) homogeneous cubes were prepared by the two-step procedure. In the first step, the $MnCO_3$/Carbon ($MnCO_3$/C) precursor was synthesized by the following process: 0.6 g of glucose was dissolved in 80 mL of 0.05 mol L^{-1} $KMnO_4$ aqueous solution with vigorously magnetic stirring followed by transferring the reaction mixtures to a 100 mL Teflon cup. The Teflon-lined autoclave was sealed and heated at 140 ^oC for 14 h. The following reaction occurred along with the carbonization of glucose:

$24KMnO_4 + 5C_6H_{12}O_6 = 24MnCO_3 + 6K_2CO_3 + 12KOH + 24H_2O$,

After heating, the Telflon-lined autoclave was cooled naturally to room temperature, and the precipitates were collected by centrifugation, washed with distilled water and absolute ethanol until the color of the supernatant became clear, and then dried overnight at 80 °C to obtain the $MnCO_3$/C cubes. In the second step, the products were calcined in air at 550 °C with a heating rate of 1 $°C\cdot min^{-1}$ for 4 h. The Mn_2O_3 phase was formed via decomposition of $MnCO_3$ along with the oxidation of Mn($^{2+}$), and simultaneous graphitization of the amorphous carbon. The final products constituted the porous Mn_2O_3/C hybrids. To control the size of the Mn_2O_3/C cubes, glucose concentration was tuned against a constant amount of $KMnO_4$. The obtained products, denoted as Mn_2O_3/C-1, Mn_2O_3/C-2, and Mn_2O_3/C-3, corresponded to 0.02, 0.04 and 0.06 mol L^{-1} of glucose respectively.

Sample Characterizations. Material masses were measured using an electronic analytical balance (AUX220, Shimadzu) with a resolution of 0.1 mg. XRD patterns were recorded on a Shimadzu XD–3A (Japan) using filtered Cu-Kα radiation (λ = 0.15418 nm) generated at 40 kV and 30 mA. Scans for 2θ values were recorded at 4° min^{-1}. Raman spectroscopy was carried out on a FT-Raman spectroscopy (RFS 100, BRUKER) employing Nd:YAG laser wave-length of 1064 nm. Scanning electron microscopy (SEM) images were obtained using a Carl Zeiss Ultra Plus. Transmission electron microscopy (TEM) high angle annular dark field scanning transmission electron microscopy (STEM) images of the catalysts were obtained using a JEOL (JEM-2000 FX) microscope operating at 200 kV. The sorption isotherms were obtained on a Quantachrome Autosorb-1 volumetric analyzer. Specific surface area was determined by Brunauer-Emmett-Teller (BET) and the pore size distribution (calculated from the desorption part of the nitrogen sorption isothers based on Barrett-Joyner-Halenda (BJH) theory) was determined from the meso and macro-range of pore size distribution. X-Ray Photoelectron Spectroscopy (XPS) spectra were generated using a PHI-5702 multifunctional X-ray photoelectron spectrometer (American). The elemental analysis of carbon(C) were conducted using an organic elemental analyzer (Thermo Flash2000).

Electrochemical measurements. Cyclic voltammetry (CV) and galvanic charge/discharge cycling was used to evaluate the electrochemical behavior of the as-prepared Mn_3O_2/C samples in a three-electrode cell system. The working electrode was fabricated using a homogeneous dough of Mn_2O_3/C, carbon black and poly(tetrafluoroethylene) of a mass ratio of 80:10:10 in isopropanol, that was rolled to uniform film thickness (~100 □m) and dried at 80 °C for 6 h. The films slices were pressed into the stainless steel grids (1 cm × 1 cm) using a tablet press. The weight of Mn_2O_3/C on the electrode was 10 mg. The reference electrode was an Hg/Hg_2SO_4 (1.0 M K_2SO_4) electrode. The electrolyte was a 1.0 mol L^{-1} Na_2SO_4. Cyclic voltammetry (CV) tests were carried out over a −0.654 V and 0.146 V (0 ~ 0.8 V *vs*. SHE) voltage range at different scan rates of 2, 5, 10, 20 and 50 mV s^{-1} using a CHI 650D electrochemical workstation. Galvanic charge/discharge and a cycle life tests were carried out on a Neware Battery Tester (BTS6.0, Neware Technology Company, Guangdong, China).

The capacitance (C) of the electrodes was calculated according to the following equation based on CVs or the discharge curves.

$$C = \frac{Q}{V} = \int \frac{i \bullet t}{V \bullet m} \qquad (1)$$

where *i* is a sampled current, *t* is a sampling time span, *V* is the total potential deviation of the voltage window, and m is the mass of the Mn_2O_3/C samples on the electrode.

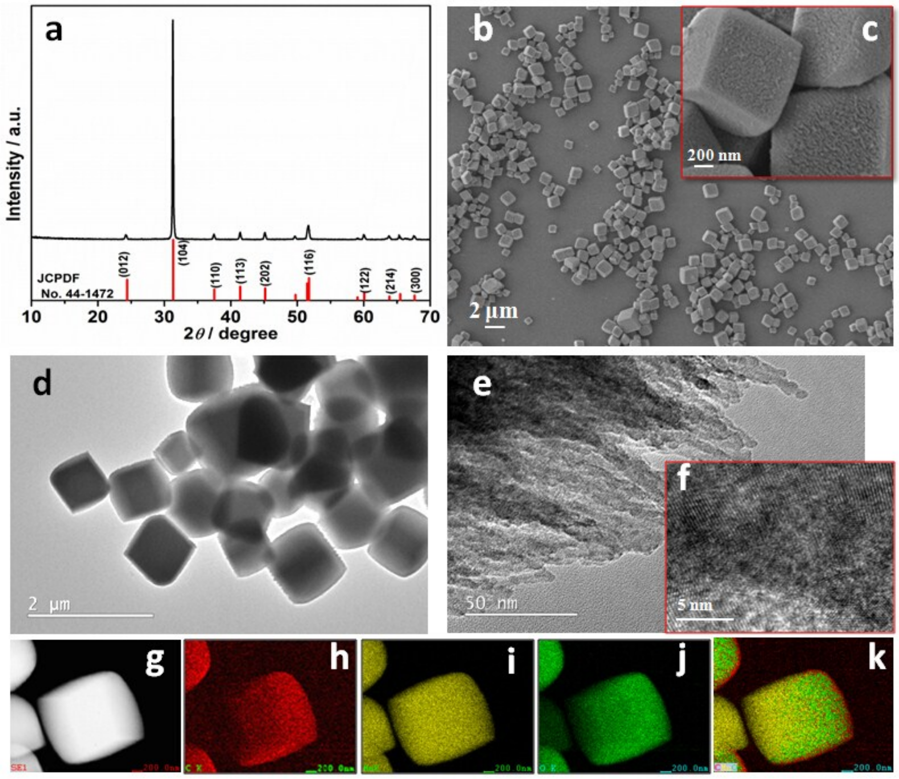

Fig. S1 (a) XRD pattern, (b,c) SEM, (d-f) TEM, (g) STEM, elemental mapping images of C (h), Mn (i) and O (j), and the overlapped elemental mapping image of $MnCO_3/C$ precursor (k).

Fig. S1a shows the crystallographic structure of the $MnCO_3/C$ precursor examined by powder X-ray diffraction (XRD). All the identified diffraction peaks unambiguously assigned to rhombohedral phase $MnCO_3$ (JCPDS Card No. 44–1472). The scanning electron micrograph (SEM) (Fig. S1b) and transmission electron micrograph (TEM) (Fig. S1d) show the uniform cube-like morphology of the particles, which had a size range estimated at ca. 500 nm-1.5 μm. The enlarged SEM image (Fig. S1c) and TEM image (Fig. S1e) shows the cubes had a dense thorny surface. The high resolution TEM (HRTEM) (Fig. S1f) shows clear lattice fringes of 0.22 nm, which relate to the (420) plane of rhombohedral $MnCO_3$. In addition, regions without visible lattice fringes can be observed in the HRTEM image. We inferred that these regions relate to the phase of amorphous carbon because the amount of the added glucose was in excess of that required for the reduction of $KMnO_4$ (see Experimental), and thus the excess glucose was carbonized under the hydrothermal conditions. The chemical microstructure of the cubes was examined using electron energy loss spectroscopic mapping. Fig. S1g shows the STEM image of a cube. Fig. S2h–j shows the uniform distribution of C, Mn, and O elements in the cube respectively. The overlapped mapping images in Fig. S1k indicate the surfaces of the cubes were covered by carbon.

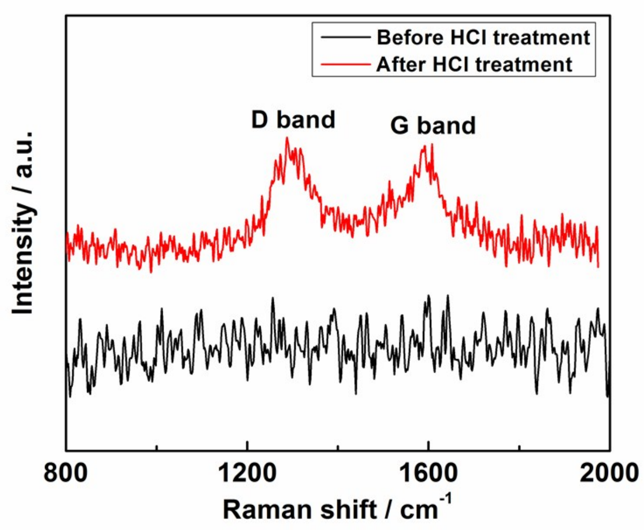

Fig. S2 Raman spectra of Mn_2O_3/C-2 sample before and after treatment with HCl.

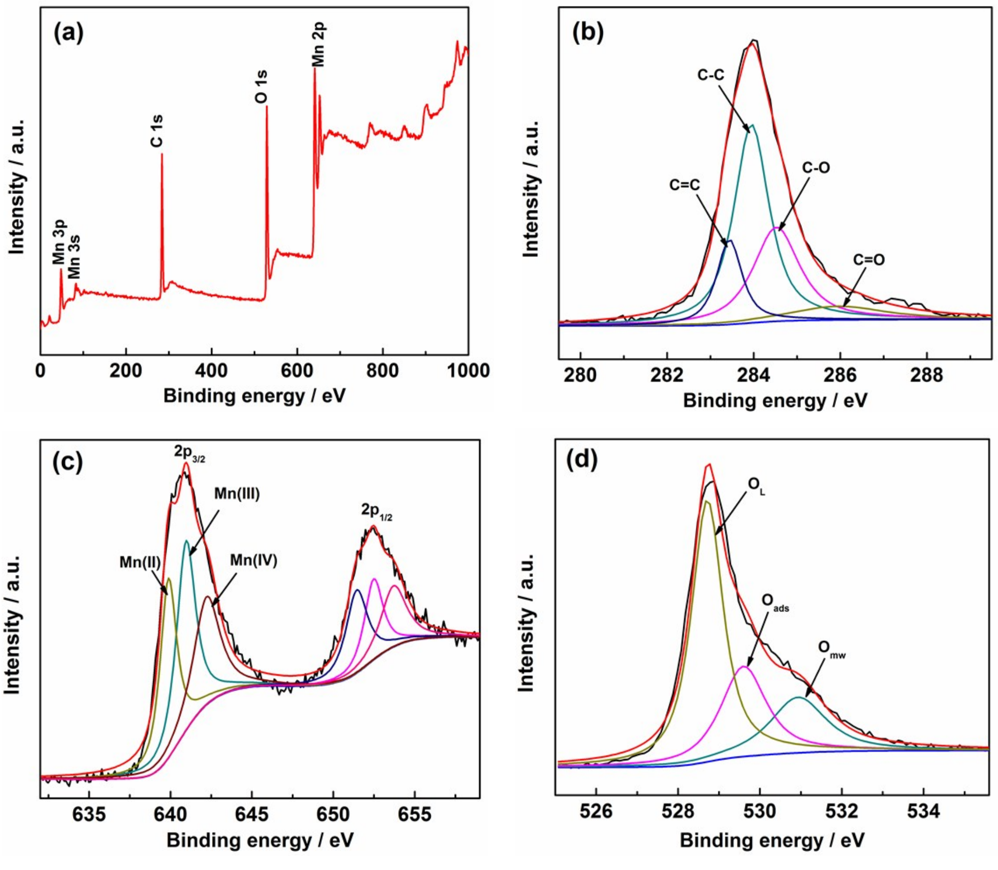

Fig. S3. (a) XPS survey, (b) C 1s, (c) Mn 2p, (d) O 1s XPS spectra of the Mn2O3/C-2 sample.

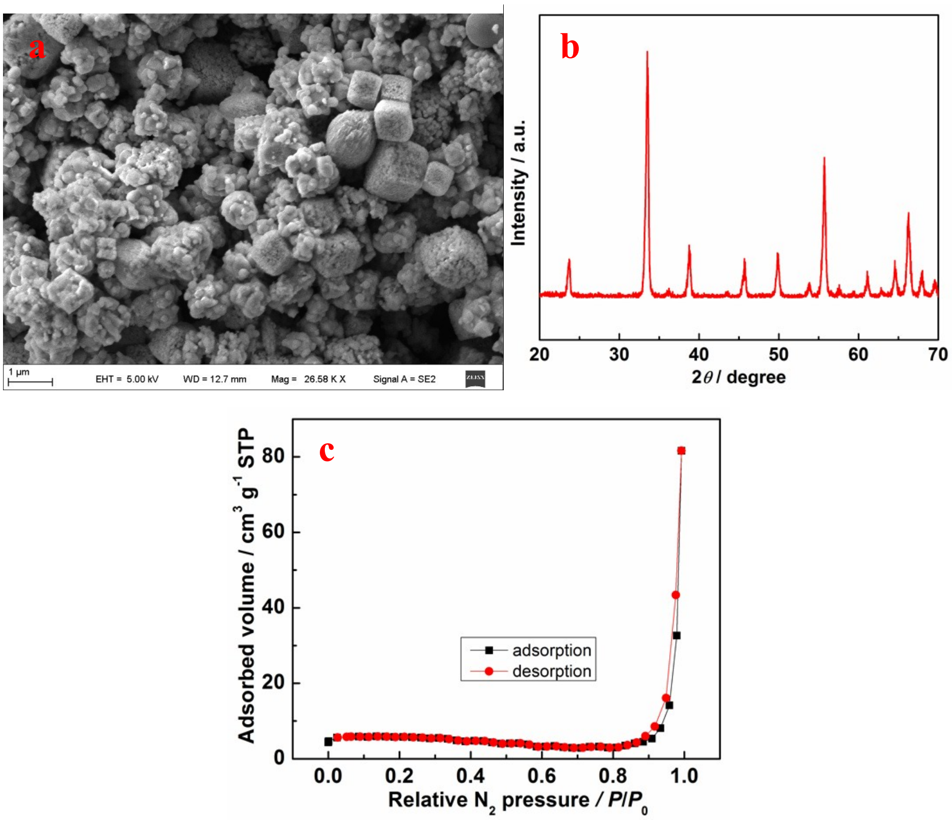

Fig. S4 (a) SEM image, (b) XRD pattern and (c) N_2 isotherm of the Mn_2O_3/C sample prepared in N_2 atmosphere. The preparation procedure was the same as that for Mn_2O_3/C-1, but calcination was in N_2 atmosphere.

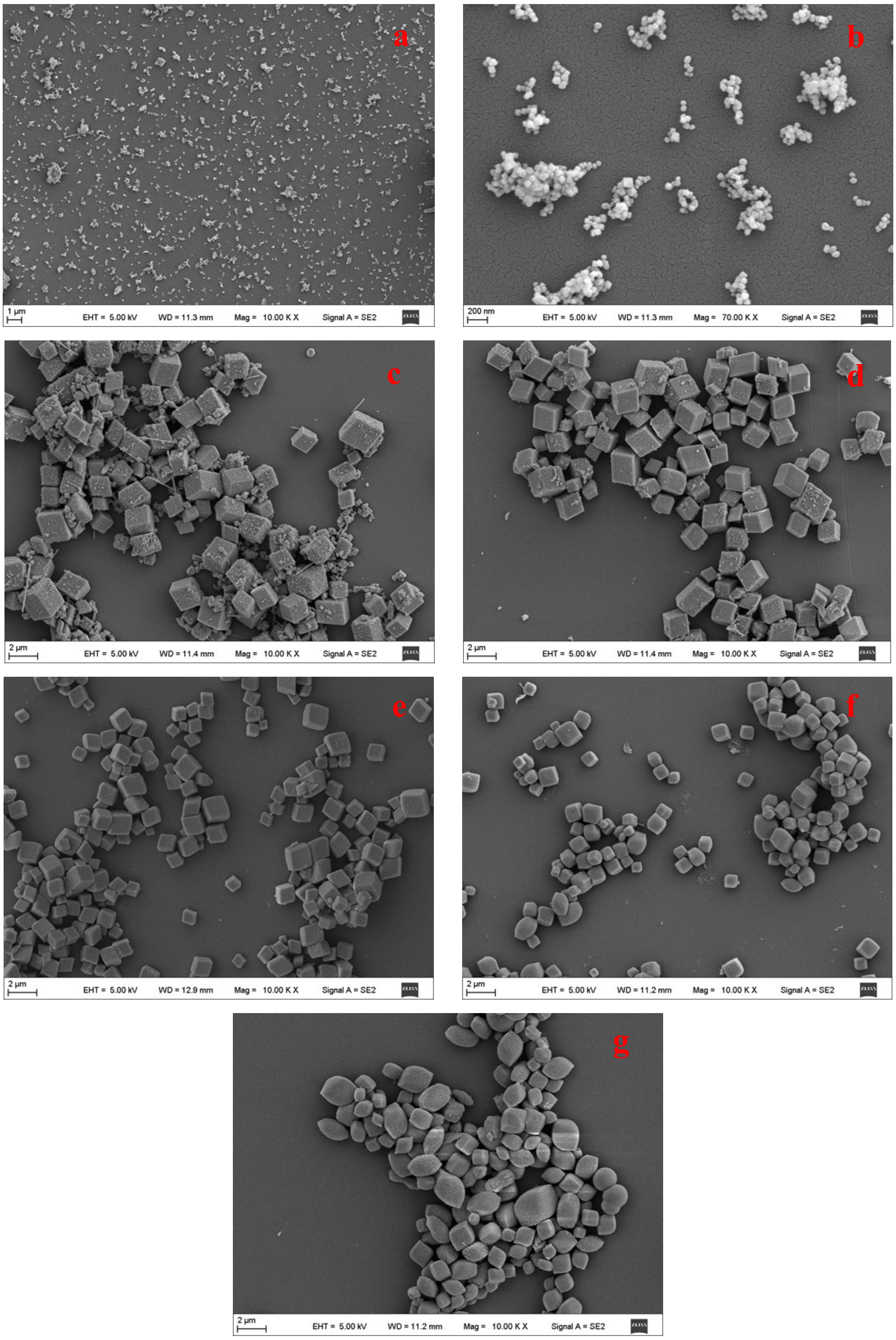

Fig. S5 SEM images of the $MnCO_3/C$ precursors prepared with different concentrations of $C_6H_{12}O_6$ at 0.015 (a,b), 0.02 (c), 0.03 (d), 0.04 (e), 0.06 (f) and 0.09 (g) mol L^{-1}.

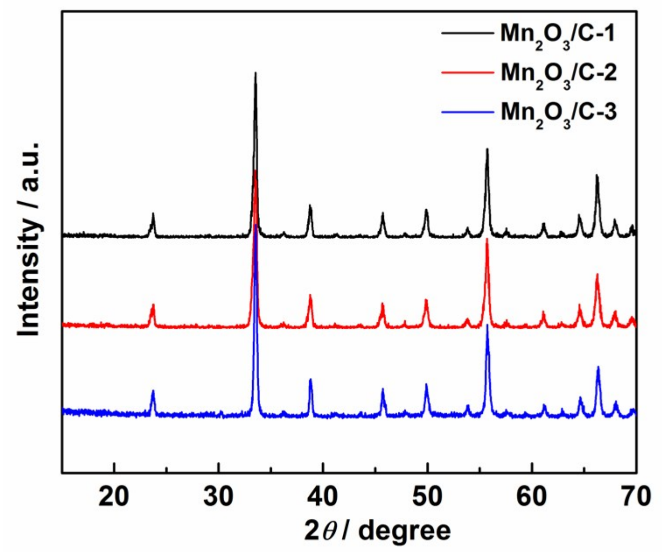

Fig. S6 XRD patterns of the Mn$_2$O$_3$/C-1 and Mn$_2$O$_3$/C-3; For comparison, the XRD pattern of Mn$_2$O$_3$/C-2 is also presented here.

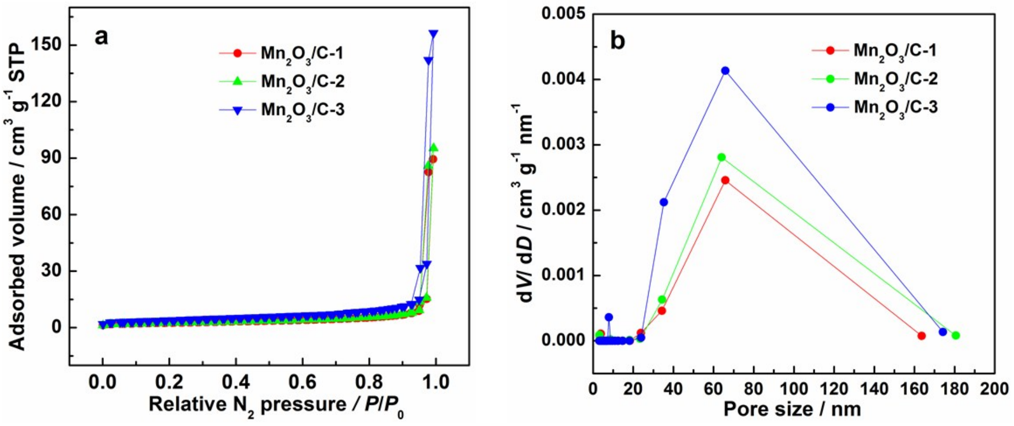

Fig. S7 (a) N$_2$ isotherms, and (b) the corresponding pore size distribution of the Mn$_2$O$_3$/C-1, Mn$_2$O$_3$/C-2, and Mn$_2$O$_3$/C-3.

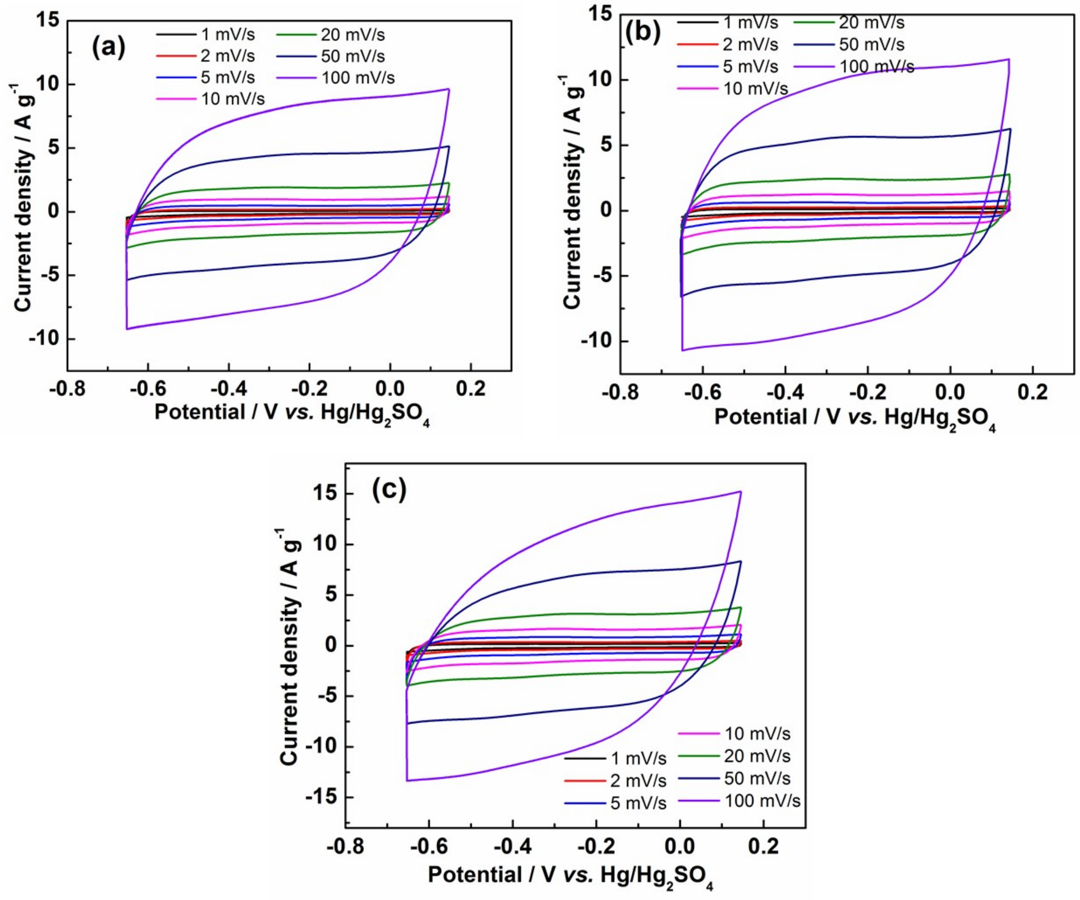

Fig. S8 CV curves of Mn_2O_3/C-1(a), Mn_2O_3/C-2 (b), and Mn_2O_3/C-3 (c) at different scan rates from 1 mV s^{-1} to 100 mV s^{-1} in 1 mol L^{-1} Na_2SO_4 solution.

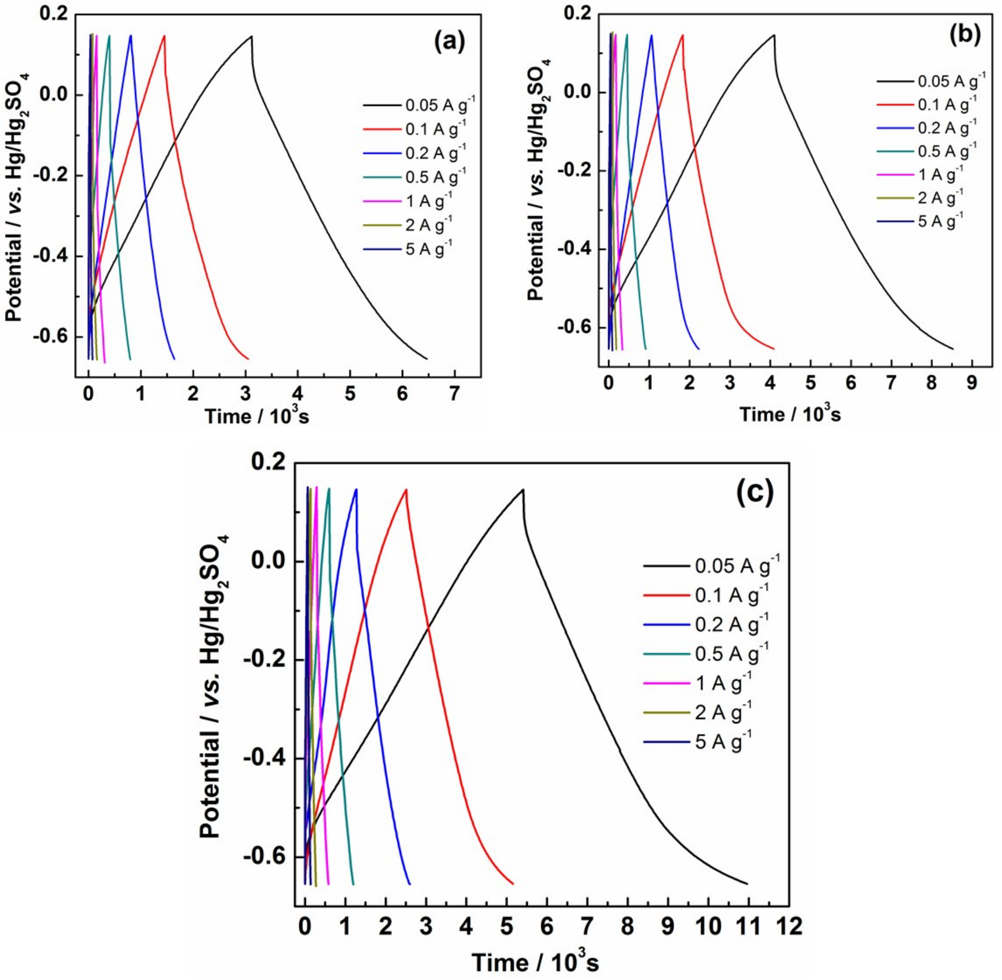

Fig. S9 Galvanic charge–discharge plots of Mn_2O_3/C-1 (a), Mn_2O_3/C-2 (b), and Mn_2O_3/C-3 (c) at different current densities of 0.05-5 A g^{-1}.

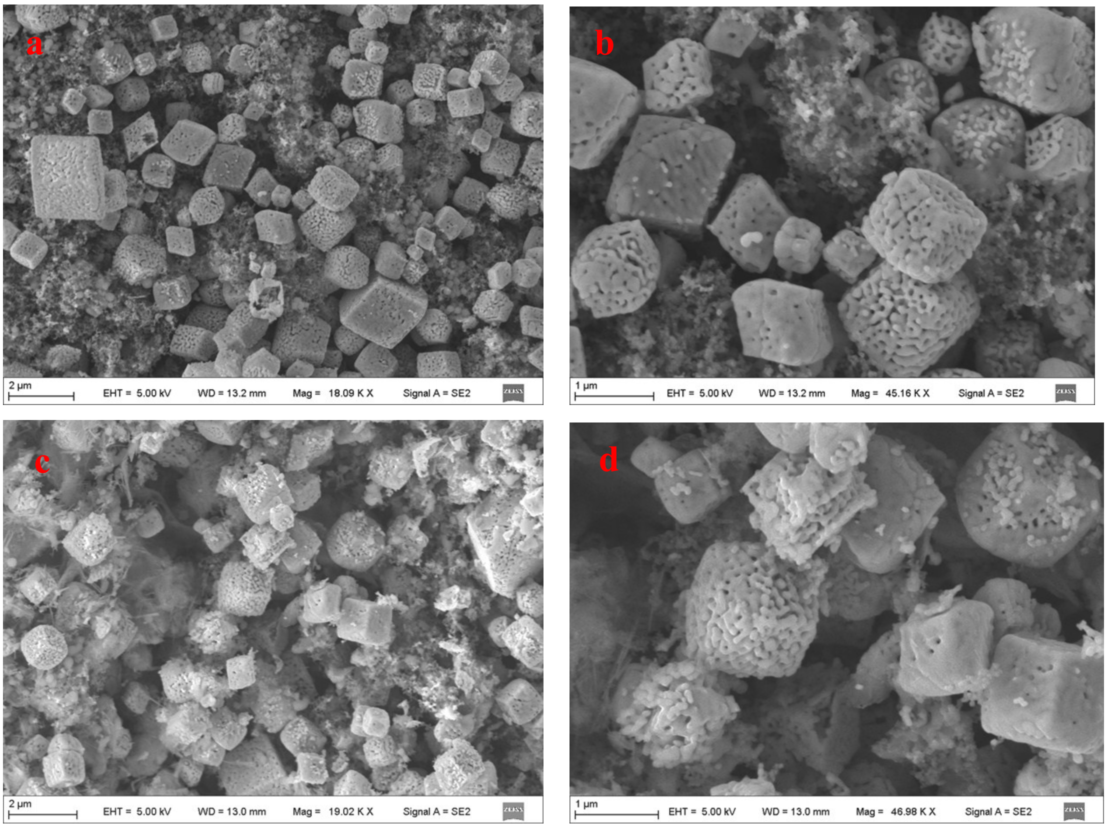

Fig. S10 SEM images of Mn_2O_3/C-2 electrode before (a,b) and after (c,d) 2000 cycles.